Charge, orbital, and magnetic ordering in $La_{0.5}Ca_{0.5}MnO_3$

P. G. Radaelli
Institut Max Von Laue-Paul Langevin, Boîte Postale 156, 38042 Grenoble Cedex 09, France

D. E. Cox
Department of Physics, Brookhaven National Laboratory, Upton, New York 11973

M. Marezio
MASPEC-CNR, via Chiavari 18A, 43100 Parma, Italy
and AT&T Bell Laboratories, Murray Hill, New Jersey 07974

S-W. Cheong
AT&T Bell Laboratories, Murray Hill, New Jersey 07974
(Received 21 June 1996)

The unusual magnetic properties of $La_{0.5}Ca_{0.5}MnO_3$ were found to be associated with structural and magnetic ordering phenomena, resulting from the close interplay between charge, orbital, and magnetic ordering. Analysis of synchrotron x-ray and neutron powder diffraction data indicates that the anomalous and hysteretic behavior of the lattice parameters occurring between $T_C \sim 225$ K and $T_N \sim 155$ K is due to the development of a Jahn-Teller (J-T) distortion of the MnO_6 octahedra, the d_z^2 orbitals being oriented perpendicular to the orthorhombic b axis. We observed an unusual broadening of the x-ray Bragg reflections throughout this temperature region, suggesting that this process occurs in stages. Below T_N, the development of well-defined satellite peaks in the x-ray patterns, associated with a transverse modulation with $q=[1/2-\varepsilon,0,0]$, indicates that quasicommensurate ($\varepsilon \sim 0$) orbital ordering occurs within the a-c plane as well. The basic structural features of the charge-ordered low-temperature phase were determined from these satellite peaks. The low-temperature magnetic structure is characterized by systematic broadening of the magnetic peaks associated with the ''Mn^{+3}'' magnetic sublattice. This phenomenon can be explained by the presence of magnetic domain boundaries, which break the coherence of the spin ordering on the Mn^{+3} sites while preserving the coherence of the spin ordering on the Mn^{+4} sublattice as well as the identity of the two sublattices. The striking resemblance between these structures and the structural ''charge ordering'' and ''discommensuration'' domain boundaries, which were recently observed by electron diffraction and real-space imaging, strongly suggests that these two types of structures are the same and implies that, in this system, commensurate long-range charge ordering coexists with quasicommensurate orbital ordering. [S0163-1829(97)05705-6]

INTRODUCTION

The close interplay between magnetism and transport properties in $A_{1-x}A'_xMnO_3$ manganese perovskites (A=La, rare earth, A'=Ca, Sr, Ba) (Ref. 1) has recently been the subject of intense research. As a function of temperature, doping, applied pressure, and A-site ionic radius, these systems display various magnetic and crystallographic transitions, some of which are associated with sharp changes of the electrical conductivity. In particular, much attention has been concentrated on the paramagnetic-to-ferromagnetic transition, for $x \sim 0.3$, associated with a sharp drop of resistivity.[2–5] The Curie temperature can be increased in a magnetic field, thereby producing a colossal magnetoresistance (CMR), traditionally ascribed to a double exchange mechanism.[6–8] The solid solution $La_{1-x}Ca_xMnO_3$ is particularly interesting, since it provides the opportunity of studying the effect of electronic doping throughout the whole range $0 \leqslant x \leqslant 1$ (corresponding to all formal Mn valences from Mn^{+3} and Mn^{+4}), with only a small variation of the ratio between A- and B-site ionic radii.[1–5,9] In 1955, Wollan and Koehler described in a classic study the several magnetic structures displayed by this system as a function of x, as determined by neutron powder diffraction.[10] In the light of this work, Goodenough proposed a comprehensive qualitative interpretation of the correlation between magnetism and transport in this system.[11] The $x=0$ end member of the solid solution, $LaMnO_3$, is an insulator at all temperatures and its low-temperature magnetic structure, which may be dependent on small variations of the La/Mn ratio, has been variously reported as ferromagnetic, antiferromagnetic, a domain mixture of the two, or spin-canted. Between $0.2<x<0.45$, the system is a ferromagnetic metal at low temperatures, and displays CMR effects near T_C. At higher doping levels ($x>0.50$) the system is antiferromagnetic at low temperatures and, in a narrow region of composition around $x=0.50$, a competition between the two types of magnetic ordering is observed.[7] At high temperatures, $La_{0.5}Ca_{0.5}MnO_3$ is a paramagnetic insulator and upon cooling, it first becomes ferromagnetic ($T_C \sim 225$ K) and then antiferromagnetic ($T_N \sim 155$ K). This intriguing behavior has been attributed to the competition between ferromagnetic double exchange and antiferromagnetic superexchange coupling. The magnetic structure of $La_{0.5}Ca_{0.5}MnO_3$, first reported by Wollan and Koehler, is

quite complex: it entails a quadrupling of the volume of the original orthorhombic unit cell and consists of two magnetic sublattices with independent propagation vectors. This observation, along with the fact that $La_{0.5}Ca_{0.5}MnO_3$ is an insulator at low temperatures, has led to the hypothesis, first formulated by Goodenough,[11] that the two sublattices result from *charge* ordering between Mn^{+3} and Mn^{+4}. In Goodenough's model, charge ordering is accompanied by *orbital ordering*, whereby the d_z^2 Mn^{+3} orbitals [associated with long Mn^{+3}-O bonds in the Jahn-Teller (J-T) distorted $Mn^{+3}O_6$ octahedra] would order, forming zig-zag chains in the a-c plane. Goodenough proposed that this ordering would entail displacements of the $Mn^{+4}O_6$ octahedra along the orthorhombic [101] direction. Very recently, the presence of a low-temperature phase transition in $La_{0.5}Ca_{0.5}MnO_3$ has been evidenced by electron diffraction (ED), by the observation of satellite reflections associated with a quasicommensurate structural modulation.[12] We have previously reported an account of the observation of structural anomalies between T_C and T_N, which are associated with the development, with decreasing temperature, of a strong J-T-type distortion of the MnO_6 octahedra. In this work, more complete structural and magnetic data on $La_{0.5}Ca_{0.5}MnO_3$, as obtained from high-resolution synchrotron x-ray and neutron powder diffraction measurements, will be presented. In particular, we show that the development of magnetic ordering is associated with the appearance of weak extra reflections in the x-ray diffraction patterns, which are the signature of small structural distortions due to *charge* and *orbital* ordering. These peaks can be indexed on a quasicommensurate superstructure with $q=[1/2-\varepsilon,0,0]$, allowing the structural parameters of the charge- and orbital-ordered phase to be refined. We have found that, in agreement with Goodenough's hypothesis,[11] the superstructure is characterized by a large J-T distortion of the $Mn^{+3}O_6$ octahedra, while the $Mn^{+4}O_6$ octahedra remain almost undistorted. Furthermore, *orbital* ordering occurs by a displacement of the $Mn^{+4}O_6$ octahedra mainly along the [0,0,1] direction (*transverse* modulation), which is in disagreement with Goodenough's early speculations.[11] Using neutron powder diffraction, we have also studied in detail the antiferromagnetic structure of $La_{0.5}Ca_{0.5}MnO_3$ at 1.5 K. By employing a high-resolution configuration, we have observed a systematic peak broadening of the magnetic reflections, which indicates that the two magnetic sublattices have quite different coherence lengths. Both the incommensurability of the structural modulation and the selective peak broadening of the magnetic reflections can be explained by the presence of a single domain boundary, which breaks the coherence of orbital ordering and of the Mn^{+3} magnetic sublattice, while leaving charge ordering and the Mn^{+4} magnetic sublattice unperturbed.

EXPERIMENTAL DETAILS

The synthesis procedure for the $La_{0.5}Ca_{0.5}MnO_3$ sample is described elsewhere.[9] Synchrotron x-ray powder diffraction data were collected on the X7A beamline at the National Synchrotron Light Source at Brookhaven National Laboratory, using a wavelength of 0.7015 Å. Two different instrument configuration were employed in the course of these experiments. On the first set of measurements, which were briefly described in Ref. 13, a narrow capillary (0.3-mm diameter) sample and a linear position-sensitive detector (PSD), with an instrumental resolution of ~0.05°, were used. Extended data sets up to $2\theta=72°$ were collected at 300, 160, and 20 K on cooling, at a wavelength of 0.7015 Å. Because of the unexpectedly complicated nature of the 160-K pattern, additional scans were performed at various temperatures over selected regions, at a wavelength of 0.7104 Å,[14] with a Ge(220) analyzer crystal inserted in the diffracted beam, giving a much better instrumental resolution of ~0.01°. In order to improve counting statistics and obtain accurate lattice parameters, a further set of data was collected as a function of temperature in the latter configuration with a flat-plate sample in symmetric reflection geometry at a wavelength of 1.1418 Å. Extended data sets were obtained at 250 and 18 K out to 2θ values of 61° and 51°, respectively.

Neutron diffraction data were collected on the high-resolution powder diffractometer D2B at the Institut Laue-Langevin in Grenoble, France. Once again, two instrument configurations were employed. Using a wavelength of 1.594 Å, in the high-intensity mode, with no primary beam collimation [the monochromator mosaic spread full width at half maximum (FWHM) being ~15′ of arc] and 5′ collimation between sample and detector, full diffraction patterns ($5°\leqslant 2\theta \leqslant 165°$) were collected at several temperatures between 1.5 and 300 K on warming. In order to obtain more detailed information on the magnetic structure, an additional diffraction pattern was collected in a higher resolution configuration. We employed a wavelength of 2.400 Å, that was filtered using a 3-cm-thick highly oriented pyrolitic graphite filter in the primary beam ($\lambda/2$ and $\lambda/3$ contamination were lower than 0.1% and 0.2%, respectively). Furthermore, the monochromatic beam divergence α_2 was limited to ~0.2°, by means of a slit system positioned ~15 cm after the monochromator (the same configuration as for the $\lambda=1.594$ data was used for the primary beam and detector collimation). This allowed a resolution of $\Delta 2\theta \approx 0.2°$ to be attained in the angular range where magnetic reflections are strongest ($2\theta \leqslant 100°$). The complete x-ray and neutron patterns were analyzed using the GSAS program.[15] Magnetization was measured using a commercial superconducting quantum interference device magnetometer and resistivity was measured by a standard four-contact ac method.

SYNCHROTRON X-RAY DIFFRACTION

Analysis of the full patterns and of individual reflections reveals that $La_{0.5}Ca_{0.5}MnO_3$ is metrically orthorhombic (i.e., $a\neq b\neq c$, $\alpha=\beta=\gamma=90°$) at all temperatures. These lattice constants are related to the simple perovskite lattice parameter a_p by $a\approx c\approx\sqrt{2}a_p$ and $b\approx 2a_p$. The systematically absent reflections are consistent with the proposed space group $Pnma$ (No. 62).[16] Below ~180 K, a few extra reflections were observed, which could not be indexed on the basis of the original unit cell (see below). As already noted,[13] the lattice parameters display large changes in the region between T_C and T_N, with a drastic decrease of the b axis and a corresponding increase of the a and c axes. Furthermore, the lattice parameters display significant hysteresis between heating and cooling runs (Fig. 1). The presence of hysteresis in this temperature range has already been evidenced by

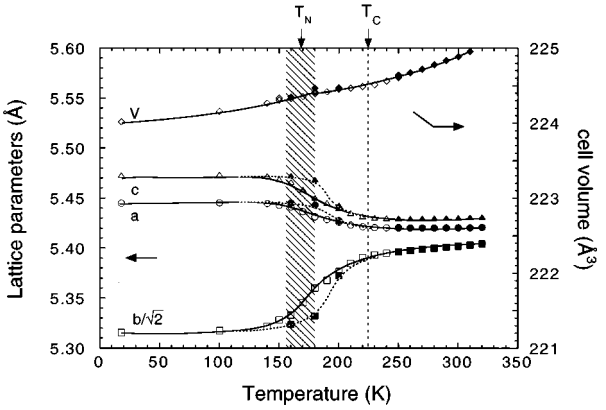

FIG. 1. Lattice parameters and unit-cell volume as a function of temperature for $La_{0.5}Ca_{0.5}MnO_3$ as obtained from synchrotron x-ray diffraction data collected at $\lambda = 1.1418$ Å. Empty and filled symbols (joined with continuous and dotted lines as guides for the eye) indicate data obtained on cooling and heating, respectively. Error bars are smaller than the symbols. The shaded area represents the width of the magnetization hysteresis loop.

magnetization and electron diffraction measurements.[9,12] The cell volume is not hysteretic and shows only a small change of slope near T_N. The region of largest change of the lattice parameters is characterized by a very unusual peak broadening effect, which we have interpreted as either a continuous distribution of lattice parameters with several maxima, which evolves with temperature, or as a number of discrete phases, each having a coherence length larger than the intrinsic coherence length for x rays (a few thousand Å), their relative proportions varying with temperature.[13] This peculiar effect deserves to be discussed in further detail. The Bragg peaks are quite sharp at room temperature and low temperatures but, between 250 and 180 K, they develop a pronounced structure, which is inconsistent with a symmetric particle size or strain effect. In our x-ray diffraction patterns, the very asymmetric peak broadening is best monitored by observing the appearance of extra scattering density between pairs of $[h\ 0\ h]$-$[0\ 2h\ 0]$ reflections (Fig. 2), the intensities of which are roughly in a 2:1 ratio (since they arise from the splitting of the $[h\ 0\ 0]$ reflection of the ideal cubic perovskite). In Fig. 2, portions of a full-pattern Rietveld refinement profile for $La_{0.5}Ca_{0.5}MnO_3$ at 160 K are shown for the [202]-[040] and [404]-[080] Bragg peaks. It is noteworthy that, apart from the better instrumental resolution of the higher order reflections and the presence of an extra peak due to accidental degeneracy, the same profile is qualitatively reproduced in the two instances, implying that the two patterns are related by a *single* scale factor. This is consistent with either a multiphase model (in our case, four phases were employed for the fit) or on any strain-type model, since the profile reflects the distribution of lattice parameters and therefore depends only on the direction (and not on the magnitude) of the reciprocal lattice vectors. We conclude that the observed effect unequivocally indicates a distribution of lattice parameters in the sample. Since, as we shall see, the large anomaly of the lattice parameters is due to the development of a static J-T distortion of the $Mn^{+3}O_6$ octahedra, the different ''phases'' may correspond to domains with different degrees of orientational orbital ordering of the J-T-

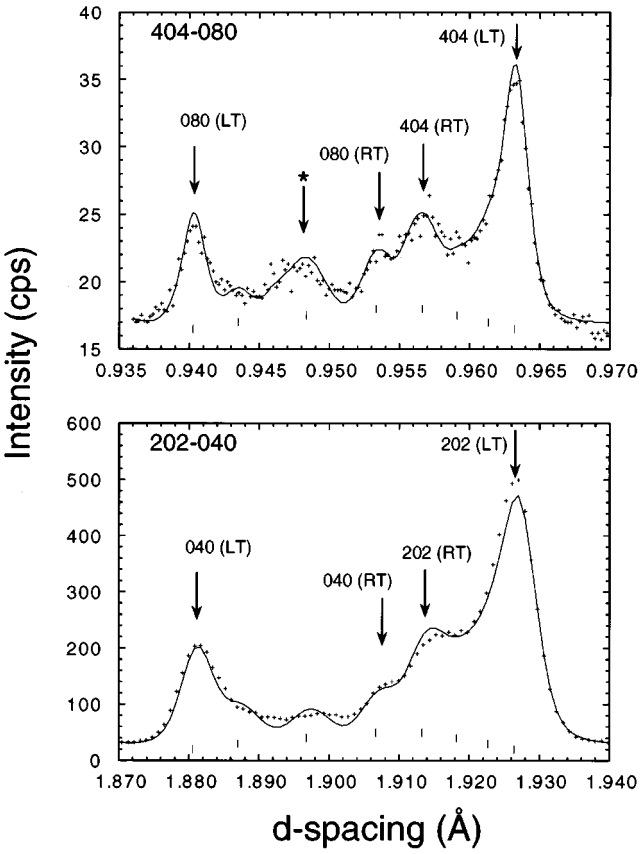

FIG. 2. Portions of a full-pattern synchrotron x-ray Rietveld refinement pattern for $La_{0.5}Ca_{0.5}MnO_3$ at 160 K ($\lambda = 0.7015$ Å), including the 202-040 (lower) and 404-080 (upper) Bragg reflections. The observed data points are indicated with crosses (+), while the calculated pattern is shown as a continuous line. The positions of the two reflections at 300 and 20 K are indicated with arrows, while those for the four phases employed in the refinements (see text) are indicated with tick marks below the patterns. The arrow with an asterisk (*) marks the position of a group of Bragg reflections with are accidentally degenerate with the 404-080 doublet but are absent for the 202-040.

distorted octahedra. This effect may be related to the development of an incommensurate structural modulation (see below).

The existence of charge ordering at low temperatures is one of the main questions to be investigated by diffraction. The observation of two independent magnetic sublattices by neutron powder diffraction[10] has been interpreted as an indication of charge disproportionation between Mn^{+3} and Mn^{+4}, which would necessarily entail a reduction of the crystallographic symmetry from $Pnma$ at least to $P2_1/m$ (with the same unit cell), since there must be two inequivalent Mn sites in the unit cell. However, the appearance of new Bragg reflections would be associated not so much with the different charge on the two sites, as with the displacement of the cations and coordination oxygen atoms, due to the different ionic radii of the two species and the presence of J-T distortion of the $Mn^{+3}O_6$ octahedra. As a consequence, in this particular instance, diffraction is much more sensitive to *orbital ordering* than to *charge ordering*. Since the smallest nuclear unit cell consistent with the magnetic symmetry would result in a doubling of either the *a* or the *c*

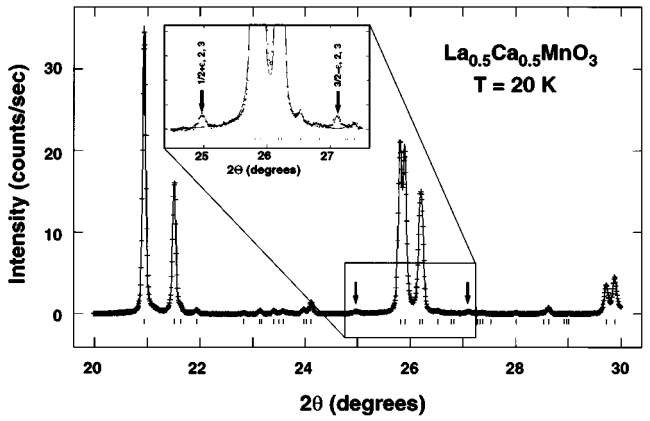

FIG. 3. Portion of an x-ray synchrotron diffraction pattern for $La_{0.5}Ca_{0.5}MnO_3$ at 20 K. The experimental points are indicated as crosses (+). The continuous line is a Le Bail (Ref. 22) fit to the pattern, obtained using the Bragg reflections (indicated by tick marks) generated by the *Pnma* space group ($a \approx c \approx \sqrt{2}a_p$ and $b \approx 2a_p$). The presence of two satellite peaks (see text for the indexing) is evidenced in the inset.

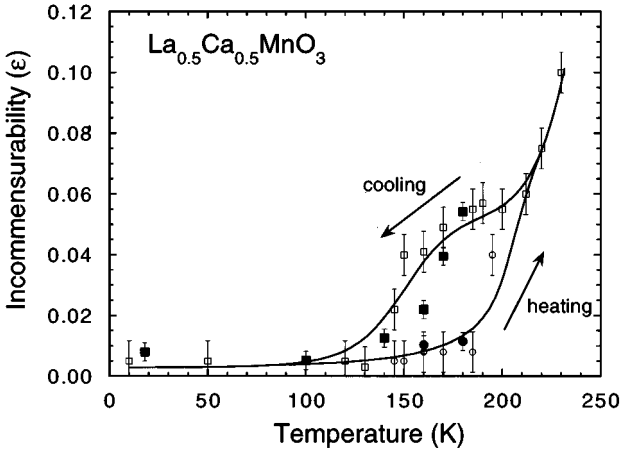

FIG. 4. Incommensurability parameter ε of the superlattice wave vector $[1/2-\varepsilon,0,0]$ as a function of temperature for $La_{0.5}Ca_{0.5}MnO_3$, as obtained from x-ray synchrotron diffraction data at $\lambda = 1.1418$ Å (filled symbols) and, for comparison, from electron diffraction (open symbols, replotted from Ref. 12). Circles and squares are heating and cooling runs, respectively. Lines are guides for the eye.

axis, Goodenough has proposed an ordering of the d_z^2 Mn^{+3} orbitals in such a way as to form zig-zag chains.[11] In fact, a few weak and rather broad reflections (~0.2° FWHM), not observed at room temperature, were seen in the 20-K pattern (Fig. 3). These are the same reflections noted in our previous papers and are significantly broadened compared to the fundamental peaks. The positions of these reflections do not exactly coincide with those predicted on the basis of a unit cell with a or c doubled, indicating that the superstructure cannot be commensurate. For example, the superlattice peak at ~27° in Fig. 3 is displaced about 0.03° to the left of the $(\frac{3}{2}\ 2\ 3)$ position, and another peak at 23.7° is displaced about 0.06° to the left of the $(\frac{5}{2}\ 0\ 2)$ position, well outside the experimental accuracy of ~0.005°. However, a satisfactory indexing can be obtained using a slightly incommensurate modulation wave vector $[1/2-\varepsilon,0,0]$. ε is ~0.01 at 20 K and shows a strong temperature dependence with pronounced hysteresis. These results are in excellent agreement with recently presented temperature-dependent electron diffraction (ED) data on the same system.[12] ED evidences the existence of a low-temperature phase transition, characterized by the appearance of superlattice reflections. However, the modulation wave vector of the superstructure was found to be quasi- but not perfectly commensurate and to display significant variations in length between different regions of the sample, as well as hysteresis. The incommensurability ε as a function of temperature, as determined from our synchrotron x-ray diffraction data and, for comparison, from ED,[12] is shown in Fig. 4.

Some preliminary remarks can be made on the basis of the positions and intensities of the observed superlattice reflections. First, only the $q=[1/2-\varepsilon,0,0]$ modulation wave vector (and not the $[0,0,1/2-\varepsilon]$) is observed, indicating a strong coupling between the modulation and the octahedral tilt pattern.[17] Second, no satellite peaks are observed for reflections with $k=2n+1$ and $l=0$ and, finally, the only observed peaks are associated with strong fundamental reflections to which La and Mn contribute in phase and which have reciprocal lattice vectors with a significant c^* component (e.g., 121, 202, and 123). These facts indicate that the displacements giving rise to the modulation are mainly along the c axis (*transverse* to the modulation wave vector), are in the same direction for atoms along the b axis related by a translation of $\sim[0,\frac{1}{2},0]$ and involve cations as well as possibly oxygen. On the basis of these consideration, a model of the superstructure was developed (Fig. 5). For simplicity, the superstructure is considered to be commensurate, with

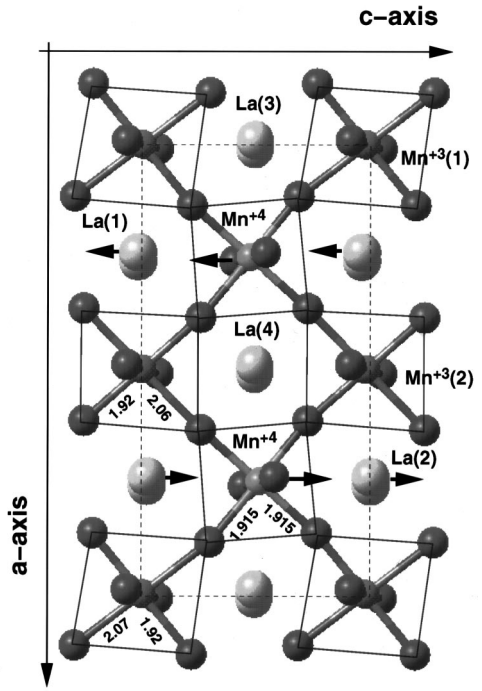

FIG. 5. Low-temperature $La_{0.5}Ca_{0.5}MnO_3$ superstructure. The projection shows the a-c plane. Arrows indicate the displacements of the $Mn^{+4}O_6$ octahedra (Δz) and of the La(1) and La(2) atoms ($\Delta z'$). Unlabeled atoms in the darkest gray shade are oxygen atoms.

TABLE I. Atomic positions for $La_{0.5}Ca_{0.5}MnO_3$ for the 20-K modulated structure, based on a doubled cell ($2a\times b\times c$) with $P2_1/m$ symmetry and Mn^{+3} atoms in special positions, La and O(1) in special positions at x, 1/4, z and Mn^{+4} and O(2) atoms in general positions at x,y,z. The least squares fit to the x-ray synchrotron data ($\lambda=1.1418$ Å) yields $\Delta z=0.018(2)$ and $\Delta z'=0.010(1)$ (see Table II). The average positional parameters were fixed to the values obtained from a Rietveld fit to the unmodulated structure with $Pnma$ symmetry, based on the same data. The numbers after the ''×'' sign indicate the site multiplicity.

Atom		x	y	z
$Mn^{+3}(1)$	×2	0.0	0.0	0.0
$Mn^{+3}(2)$	×2	0.5	0.0	0.0
Mn^{+4}	×4	0.25	0.0	$0.5-\Delta z$
La(1)	×2	0.26	0.25	$0.004-\Delta z'$
La(2)	×2	0.76	0.25	$0.004+\Delta z'$
La(3)	×2	0.01	0.25	0.496
La(4)	×2	0.51	0.25	0.496
O1(1)	×2	−0.005	0.25	−0.065
O1(2)	×2	0.495	0.25	−0.065
O1(3)	×2	0.245	0.25	$0.565-\Delta z$
O1(4)	×2	0.745	0.25	$0.565+\Delta z$
O2(1)	×4	0.1375	0.034	$0.235-\Delta z$
O2(2)	×4	0.6375	0.034	$0.235+\Delta z$
O2(3)	×4	0.1175	−0.034	$0.725-\Delta z$
O2(4)	×4	0.6175	−0.034	$0.725+\Delta z$

$a\approx 2\times\sqrt{2}a_p$, $c\approx\sqrt{2}a_p$, and $b\approx 2a_p$ (exact doubling along the a axis) and to have $P2_1/m$ space group symmetry.[18] This space group can be derived from the aforementioned charge-ordered subgroup of $Pnma$ ($P2_1/m$ *without* cell doubling) by removing one half of the screw axes and the corresponding centers of symmetry located on the Mn^{+4} atoms (the reason for the Mn^{+4} and Mn^{+3} labeling will be clear from what follows). In the $P2_1/m$ structure, the four inequivalent atoms [Mn, La, O(1), and O(2)] in the $Pnma$ cell are distributed among fifteen sets of sites, involving a total of 31 positional parameters, as listed in Table I. Although the data are clearly inadequate for a full refinement of this structure, good results were obtained with a highly constrained model based on the average structure with $Pnma$ symmetry and the following additional features: (i) the four O(2) atoms in the a-c plane surrounding the Mn^{+4} atoms were shifted towards the latter, so as to give a roughly regular undistorted octahedron with Mn-O distances of about 1.915 Å. (ii) the $Mn^{+4}O_6$ octahedron centered at $\frac{1}{4},0,\frac{1}{2}$ was shifted along c towards the Mn^{+3} atoms at 0,0,0 and $\frac{1}{2},0,0$ by Δz, while the $Mn^{+4}O_6$ octahedron centered at $\frac{3}{4},0,\frac{1}{2}$ was shifted in the opposite direction (see Table I). (iii) the La(1) and La(2) atoms were shifted by $\Delta z'$ in the same direction as the neighboring $Mn^{+4}O_6$ octahedra. (iv) the Mn^{+3} and remaining La and O(1) atoms were left undisturbed. Integrated intensities were obtained for all possible satellite peaks which were reasonably well separated from adjacent fundamental peaks, out to $2\theta=27°$ (14 peaks in all) and a least-squares fit was carried out with two variable parameters, Δz and $\Delta z'$. The scale factor was fixed at the value determined from a Rietveld fit to the average (unmodulated) structure with $Pnma$ symmetry. The results are listed in Table II and we find the agreement to be very satisfactory in view of the simplicity of the above model. Based on the value of 0.018(2) found for Δz, Mn^{+3} has two long distances in the a-c plane [2.07 and 2.06 Å for $Mn^{+3}(1)$ and $Mn^{+3}(2)$, respectively] and four short distances averaging about 1.92 Å, entirely consistent with a J-T distortion of the $Mn^{+3}O_6$ octahedra. The shift in the associated La positions, $\Delta z'$, is only about half of Δz, and presumably reflects the less rigidly constrained coordination around the La atoms.

TABLE II. Least-squares fit of observed and calculated intensities for the 20-K modulated structure of $La_{0.5}Ca_{0.5}MnO_3$ based on the positions listed in Table I with $\Delta z=0.018(2)$ and $\Delta z'=0.010(1)$. Estimated errors for I(obs) are given in parentheses. The values of I(calc) were scaled based on a fit to the average structure with $Pnma$ symmetry.

hkl	I(obs)	I(calc)
$101,\ 10\bar{1}$	0(5)	3
$111,\ 11\bar{1}$	0(5)	0
$301,\ 30\bar{1}$	0(5)	1
$121,\ 12\bar{1}$	24(5)	26
$112,\ 11\bar{2}$	0(5)	2
$321,\ 321$	5(5)	14
$302,\ 30\bar{2}$ $122,\ 12\bar{2}$	136(50)	93
$501,\ 50\bar{1}$	0(5)	0
$132,\ 13\bar{2}$	0(5)	1
$103,\ 10\bar{3}$	0(5)	0
$502,\ 50\bar{2}$	44(10)	36
$332,\ 332$	0(10)	0
$303,\ 30\bar{3}$ $123,\ 12\bar{3}$	70(10)	56
$701,\ 70\bar{1}$ $323,\ 32\bar{3}$	40(10)	50

NEUTRON DIFFRACTION

The observation of an anomaly in the lattice parameters between T_C and T_N implies that atomic positions change significantly. This issue was investigated by refining the structural parameters using the Rietveld method. Both x-ray and neutron-diffraction data were used for this purpose, yielding the same qualitative answer, but only the neutron results will be reported in view of their higher accuracy. In addition, the complex peak broadening displayed in the region between the magnetic transitions made it difficult to obtain reliable structural parameters for the various ''phases''. Therefore, for the structural parameter determination, we used only data obtained at 300 and at 1.5 K, where the broadening effect is minimal. However, it is clear from inspection of both x-ray and neutron patterns that a small amount of untransformed material is still present at low temperature, and this was modeled in the fits as a second phase with lattice parameters close to those of the room-temperature phase and identical positional parameters. Since this ''phase'' only gives a small contribution to the total integrated intensity [6.6(2)%] and since its structural parameters were not refined during the fit, we will not discuss it in

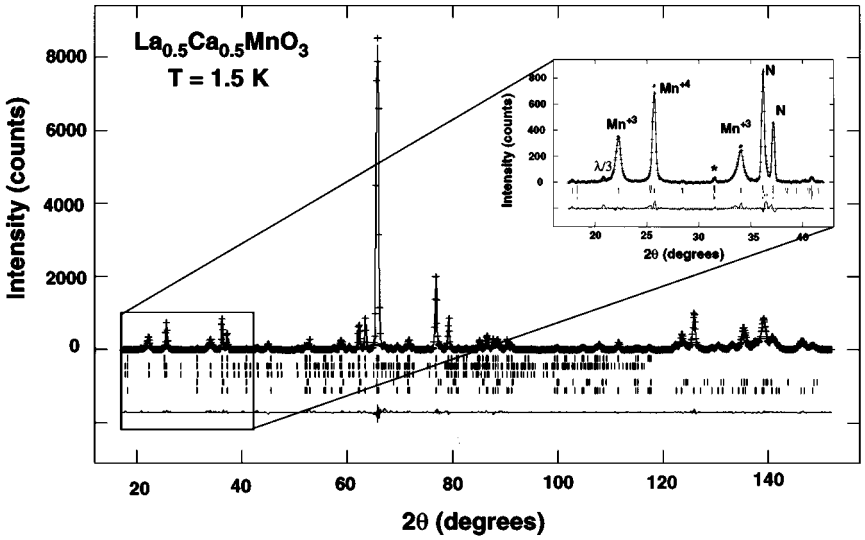

FIG. 6. Rietveld plot of $La_{0.5}Ca_{0.5}MnO_3$ neutron powder diffraction data at 1.5 K ($\lambda=2.400$ Å). Symbols are as for Fig. 2. A difference curve (observed minus calculated) is plotted at the bottom. The tick marks indicate Bragg reflections for the following phases (starting from the bottom): main nuclear phase, residual high temperature phase, Mn^{+3} magnetic phase, Mn^{+4} magnetic phase, *G*-type magnetic phase (assumed to be from the residual high-temperature phase). The inset shows a detail of the low-angle region of the pattern. To emphasize the selective broadening effect, a few nuclear Bragg peaks (N) as well as magnetic peaks from the Mn^{+3} and Mn^{+4} sublattices are labeled. The asterisk marks the position of the [110] reflection, typical of the *G*-type phase (see text).

detail. It is noteworthy, however, that this minority component of the sample may display antiferromagnetic (AFM) ordering different from that of the majority phase (see below). At low temperatures, a significant contribution to the total neutron diffracted intensity is due to magnetic reflections, especially in the low-angle region of the pattern. A preliminary set of refinements was carried out based only on the 1.594 Å data above 30°. After the determination of the details of the magnetic structure (see below), both 1.594 and 2.400 Å data were simultaneously used in the refinement procedure. On the basis of the x-ray diffraction results, we would expect the appearance of nuclear superlattice reflections in the neutron-diffraction patterns as well. In fact, the strongest nuclear peak predicted on the basis of the aforementioned quasicommensurate superstructure (1/2-ε,2,2) is visible near 67° (for $\lambda=2.400$ Å) as a small hump in the difference curve, even after accounting for all the magnetic reflections (Fig. 6). However, the scattering at the superlattice positions is dominated by the much larger magnetic reflections, leading to instabilities in the refinements based on the lower symmetry of the quasicommensurate structure, namely $P2_1/m$. Therefore, subsequent refinements based on neutron-diffraction data were carried out in the higher symmetry *Pnma* space group, characteristic of the structure above the transition. It should be clear that this procedure will yield only a structure averaged over the symmetry operators of the *Pnma* space group. The corresponding $La_{0.5}Ca_{0.5}MnO_3$ structural parameters at 300 and 1.5 K are reported in Table III and selected bond distances and angles are reported in Table IV.

The most significant difference between the room-temperature and low-temperature structures is in the Mn-O bond lengths. At room temperature, the octahedral coordination of manganese with oxygen is almost undistorted, with six equal Mn-O distances. At low temperatures, the two Mn-O(1) distances (along the *b* axis) become shorter than the four Mn-O(2) distances in the *a*-*c* plane by ~0.04 Å, implying a J-T distortion of the ''*apically compressed*'' type. This result is completely consistent with the superstructure model discussed above, as the in-plane Mn bond length, averaged over the *Pnma* symmetry operators, will yield for both Mn-O(2) bond lengths in *Pnma* essentially the same value, which will be longer than the simple Mn-O(1) ''AFM'' bond along the *b* axis, hence mimicking the presence of an ''apically compressed'' octahedron. These results clearly demonstrate that there is close link between the lattice parameters and the presence of J-T distorted $Mn^{+3}O_6$ octahedra with the d_{z^2} orbital oriented in the *a*-*c* plane. This supports the interpretation of the multiple ''phases'' with different lattice parameters observed by x-ray diffraction between T_C and T_N as different stages of the development of orientational orbital ordering. It should be remarked that conventional diffraction techniques, being sensitive to the *average* structure, are unable to unambiguously determine the nature of the high-temperature structure, which may contain either undistorted or orientationally disordered MnO_6 octahedra (either statically or dynamically). This ambiguity could be resolved only by employing techniques which are sensitive to the local structure, such as extended x-ray-absorption fine structure or pair distribution function analysis.

The magnetic reflections in the low-temperature neutron powder diffraction patterns may be indexed on the basis of the $a\approx c\approx 2\times\sqrt{2}a_p$ and $b\approx 2a_p$ unit cell, previously proposed by Wollan and Koehler.[10] The magnetic structure, known as CE-type, is characterized by two Mn sublattices. As we have seen, based on the sizes and the distortions of the octahedra on the inequivalent Mn sites in the modulated structure (orbital ordering), there is strong circumstantial evidence for charge ordering in this system. Furthermore, as we shall see in further detail, all the neutron observations are consistent with the charge ordering being *commensurate*, *long range*, and *coupled with the magnetic ordering*. As a

TABLE III. $La_{0.5}Ca_{0.5}MnO_3$ structural parameters at 300 and 1.5 K, as determined from Rietveld refinements based on neutron powder diffraction data. A single wavelength [1.59434(2) Å] was used for the 300-K data, while, for 1.5 K, data obtained at two wavelengths [1.59434(2) and 2.39979(3) Å] were simultaneously refined. The space group $Pnma$ (No. 62) was used at both temperatures (see text). The atomic sites are: La/Ca $4c[x,\frac{1}{4},z]$; Mn $4a[0,0,0]$; O(1) $4c[x,\frac{1}{4},z]$; O(2) $8d[x,y,z]$. The fractional occupancies were fixed to 0.5 (for La and Ca) and 1 for all the other atoms, and not refined. Numbers in parentheses are statistical errors in the last significant digit.

Parameter		$T=300$ K	$T=1.5$ K
a (Å)		5.4248(1)	5.4466(3)
b (Å)		7.6470(2)	7.5247(4)
c (Å)		5.4355(1)	5.4763(3)
V (Å)^3		225.485(9)	224.44(2)
La/Ca	x	0.0195(3)	0.0194(3)
	z	0.4952(4)	0.4964(2)
	U(Å^2)	0.0099(2)	0.0090(3)
Mn	U(Å^2)	0.0040(3)	0.0017(5)
O(1)	x	0.4926(4)	0.4905(4)
	z	0.5608(3)	0.5645(2)
	U_{11}(Å^2)	0.014(1)	0.0080(9)
	U_{22}(Å^2)	0.0057(6)	0.0054(7)
	U_{33}(Å^2)	0.0125(7)	0.0147(8)
	U_{13}(Å^2)	0.0008(8)	0.001(1)
O(2)	x	0.2763(2)	0.2720(2)
	y	0.0307(1)	0.0337(1)
	z	0.2236(2)	0.2271(2)
	U_{11}(Å^2)	0.0085(5)	0.0031(6)
	U_{22}(Å^2)	0.0144(4)	0.0056(4)
	U_{33}(Å^2)	0.0108(5)	0.0261(8)
	U_{12}(Å^2)	−0.0024(6)	−0.0013(8)
	U_{13}(Å^2)	−0.0045(4)	0.0010(4)
	U_{23}(Å^2)	−0.0021(7)	−0.0028(8)
R_{wp} (%)		4.54	5.85[a]
$R(F^2)$ (%) (λ=1.594)		3.69	9.46
$R(F^2)$ (%) (λ=2.400)			4.65
χ^2		5.803	6.570[a]

[a]For both histograms.

consequence, we will still label the two magnetic sublattices ''Mn^{+3}'' and ''Mn^{+4}'' as in the original paper by Wollan and Koehler.[10] The magnetic structures of the two sublattices have different propagation vectors: $[\frac{1}{2},0,\frac{1}{2}]$ for Mn^{+4} (U point of the first Brillouin zone) and $[0,0,\frac{1}{2}]$ or $[\frac{1}{2},0,0]$ for Mn^{+3} (Z or X point of the first Brillouin zone). In view of the pronounced broadening of the Mn^{+3} reflections (see below), it is not possible to resolve the ambiguity between the two propagation vectors directly from the data. However, space group considerations make it very natural for the Mn^{+3} magnetic propagation vector to be perpendicular to the structural modulation wave vector $[1/2-\varepsilon,0,0]$. In fact, in this case, the space group of the ideally commensurate structural modulation ($P2_1/m$ with $2a\times b\times c$) would coincide with the unitary group associated with the Shubnikov group of the magnetic structure ($P_{2c}2_1/m$ with $2a\times b\times 2c$ for spins in the a-c plane, as discussed below[19]). Therefore, in what follows,

TABLE IV. Selected bond distances and angles for $La_{0.5}Ca_{0.5}MnO_3$, as obtained from Rietveld refinements of neutron powder diffraction data. Numbers after the multiplication sign (×) are bond multiplicities. Estimated errors are in parentheses.

Parameter	$T=300$ K	$T=1.5$ K
Mn-O(1) (Å)×2	1.9406(3)	1.9148(3)
Mn-O(2) (Å)×2	1.944(2)	1.951(1)
	1.946(2)	1.959(1)
La/Ca-O(1) (Å)×1	2.881(3)	2.904(2)
	2.591(2)	2.593(2)
	3.026(2)	3.076(2)
	2.417(2)	2.410(2)
La/Ca-O(2) (Å)×2	2.633(2)	2.592(1)
	2.716(1)	2.728(1)
	3.085(1)	3.061(1)
	2.443(2)	2.442(2)
O(1)-Mn-O(2) (°)	89.79(7)	89.40(6)
	89.99(6)	89.81(6)
	90.21(7)	90.60(6)
	90.01(6)	90.19(6)
O(2)-Mn-O(2) (°)	90.94(1)	91.25(1)
	89.06(1)	88.75(1)
Mn-O(1)-Mn (°)	160.23(9)	158.51(8)
Mn-O(2)-Mn (°)	161.65(6)	161.93(5)

we will assume the propagation vector of the Mn^{+3} magnetic sublattice to be parallel to the c axis. Rietveld refinements of the low-temperature neutron powder diffraction patterns clearly indicate that the magnetic moments are predominantly oriented in the a-c plane but there is a certain degree of ambiguity in the determination of the spin directions within the a-c plane. For Mn^{+3}, the x and z components of the magnetic moment could be refined separately, but the same could not be done reliably for the Mn^{+4} sublattice and the latter were therefore constrained to be parallel to the c axis. The refined values of the magnetic moments are reported in Table V. Although the CE-type structure accounts for the great majority of the magnetic reflections, at 1.5 K,

TABLE V. Refined magnetic moment components of the Mn^{+3} and Mn^{+4} sublattices, for $La_{0.5}Ca_{0.5}MnO_3$ at 1.5 K. The magnitudes of the magnetic moments are: $\mu_{Mn^{+3}}=2.98(2)$ and $\mu_{Mn^{+4}}=2.57(2)$. The site coordinates are expressed as fractions of the $2a\times b\times 2c$ magnetic cell. The Shubnikov symmetry is $P_{2c}2_1/m$ (Ref. 19).

Mn^{+3} sublattice			Mn^{+4} sublattice	
sites	μ_x	μ_z	sites	μ_z
$0\ \frac{1}{4}\ 0$	1.01(9)	2.80(4)	$\frac{1}{4}\ \frac{1}{4}\ \frac{1}{4}$	2.57(2)
$\frac{1}{2}\ \frac{1}{4}\ 0$			$\frac{3}{4}\ \frac{1}{4}\ \frac{3}{4}$	
$0\ \frac{3}{4}\ \frac{1}{2}$			$\frac{1}{4}\ \frac{3}{4}\ \frac{3}{4}$	
$\frac{1}{2}\ \frac{3}{4}\ \frac{1}{2}$			$\frac{3}{4}\ \frac{3}{4}\ \frac{1}{4}$	
$0\ \frac{1}{4}\ \frac{1}{2}$	−1.01(9)	−2.80(4)	$\frac{1}{4}\ \frac{1}{4}\ \frac{3}{4}$	−2.57(2)
$\frac{1}{2}\ \frac{1}{4}\ \frac{1}{2}$			$\frac{3}{4}\ \frac{1}{4}\ \frac{1}{4}$	
$0\ \frac{3}{4}\ 0$			$\frac{1}{4}\ \frac{3}{4}\ \frac{1}{4}$	
$\frac{1}{2}\ \frac{3}{4}\ 0$			$\frac{3}{4}\ \frac{3}{4}\ \frac{3}{4}$	

there is evidence for a small magnetic [110]/[011] reflection, which is typical of the so-called *G*-type phase, in which there is AFM coupling in all directions[10] (this peak is absent at 50 K, but is present at 1.5 K for both the 1.594 and the 2.400 Å data sets, and cannot therefore be due to λ/2 contamination). Should this additional magnetic component be attributed to the majority phase, it would correspond to $\sim 0.3\mu_B$/Mn atom. An alternative explanation, which we believe to be more likely, is that this magnetic signal should be attributed to the minority phase.

A striking feature of the $La_{0.5}Ca_{0.5}MnO_3$ magnetic structure, as revealed by the neutron powder diffraction data, is the presence of two different coherence lengths for the two magnetic sublattices. The low-angle portion of the full-pattern Rietveld refinement profile for $La_{0.5}Ca_{0.5}MnO_3$ at 1.59 K (2.400 Å data) is shown in Fig. 6. It is clear by inspection that, while the nuclear peaks and the magnetic Bragg peaks associated with the Mn^{+4} sublattice are resolution-limited, the Mn^{+3} reflections are significantly broadened. This broadening can be satisfactorily modeled using a particle-size-type Lorentzian term, from which, using the simple Scherrer formula, a magnetic domain size of ~310 Å can be calculated (or if an anisotropic model is used, ~250 and ~450 Å in the directions parallel and perpendicular to the *a* axis, respectively).[20] On the contrary, the coherence length of the Mn^{+4} magnetic sublattice is comparable to that of the nuclear structure, i.e., $\sim >2000$ Å. This result is most intriguing, since it indicates that the two interpenetrating magnetic sublattices have quite different coherence lengths and implies the presence, in the magnetic structure, of domain boundaries capable of breaking the coherence of the Mn^{+3} sublattice, while leaving the Mn^{+4} sublattice unperturbed. It is not difficult, however, to show that several such domain boundaries can exist: among them, a ''twin'' boundary, at which there is a change by 90° in the *direction* of the Mn^{+3} propagation vector with respect to the crystallographic axes and a ''spin-flip'' boundary, that reverses the directions of the spins on the Mn^{+3} sublattice. The striking similarities between these *magnetic* domain boundaries and the *structural* domain boundaries, which were recently observed by electron diffraction and imaging, strongly suggest that these structures actually coincide. Since the Mn^{+3} propagation vector is probably coupled magnetoelastically rather strongly to one of the two inequivalent in-plane crystallographic axes (*a* or *c*), the magnetic twin boundaries are likely to be associated with the structural *a*-*c* twins and also with the charge ordered domain (COD) boundaries, observed by ED.[12] On the other hand, the magnetic ''spin-flip'' boundaries are likely to coincide with the much more finely spaced *discommensuration* DC boundaries, which are responsible for the incommensurability of the structural modulation.[12] This hypothesis is confirmed by the fact that the relationship between the incommensurability ε and the domain size L ($L=2\pi/p\varepsilon$, with $p=2$ (Ref. 21) and $\varepsilon\sim 0.009$ at 20 K) would yield $L\sim 350$ Å, which is very similar to the magnetic coherence length found for the Mn^{+3} sublattice. In Fig. 7, we depict a model for such a magnetic and structural domain boundary. It can be seen that, at the domain boundary, there is no loss of coherence for the charge and magnetic ordering into ''Mn^{+3}'' and ''Mn^{+4}'' sublattices. Likewise, the spin structure of the Mn^{+4} *magnetic* lattice is not perturbed through the domain boundary. However, the directions of the spins on the Mn^{+3} sublattices are reversed, and the phase of the structural modulation wave (indicated by arrows) is abruptly changed by π. Therefore, a single type of defect is able to explain both the incommensurability of the structural modulation and the selective coherence length effects on the magnetic structure.

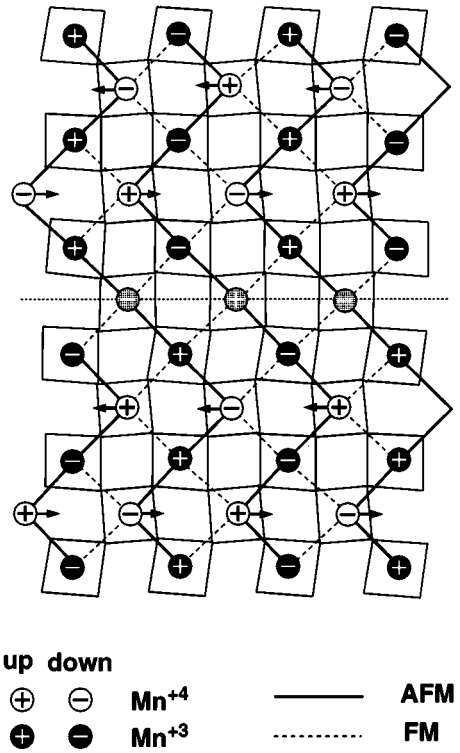

FIG. 7. Proposed model for the structural/magnetic domain boundary responsible for the incommensurability of the structural modulation and for the selective coherence lengths effects on the magnetic structure. The projection shows the *a*-*c* plane (orientation is the same as in Fig. 5). Filled and empty circles are Mn^{+3} and Mn^{+4}, respectively. Pluses (+) and minuses (−) indicate the directions of the spins (actually oriented in the same *a*-*c* plane). Arrows indicate the direction of the displacements giving rise to the structural modulation. AFM and ferromagnetic couplings are indicated with continuous and dashed lines, respectively. The domain boundary is indicated with a horizontal dotted line.

CONCLUSIONS

The early work on $La_{0.5}Ca_{0.5}MnO_3$ established a fairly simple picture of this system, in which magnetic ordering was associated with commensurate charge ordering, through a separation of Mn^{+3} and Mn^{+4} onto two interpenetrating commensurate sublattices and with commensurate orbital ordering. A comparative evaluation of our x-ray and neutron diffraction results, as well as recent ED data, clearly indicates that this scenario is oversimplified and that the true nature of this system is considerably more complex. The region between T_C and T_N is characterized by a rapid change of the lattice parameters, associated with the development of a J-T distortion of the octahedra as well as partial orbital ordering, by which the average angle between the long Mn-O bond (d_z^2 Mn orbital) and the *b* axis gradually ap-

proaches 90°. The different ''phases'' observed by x-ray diffraction (characterized by different values of the b axis) are likely to be discrete intermediate stages in this process. At the same time, ED indicates that, in the same temperature range, there is a certain degree of incommensurate orbital ordering in the a-c plane as well. Below T_N, the observation of satellite peaks by x-ray diffraction, as well as the ED and real-space imaging evidence, indicate that orbital ordering in the a-c plane locks into a quasicommensurate propagation vector at sufficiently low temperatures, characterized by the presence of phase-breaking discommensuration boundaries. Structural refinements based on the integrated intensities of the satellite peaks allow the formulation of a plausible model for the superstructure, in which the symmetry lowering is obtained by correlated displacements of cations and oxygen. The Mn atoms, which are symmetry-equivalent in the $Pnma$ structure, are distributed among three crystallographically inequivalent sites in the ideally commensurate $P2_1/m$ superstructure: for two of these sites, each having twofold multiplicity (Mn^{+3}), the coordination oxygen atoms form strongly J-T distorted octahedra, whereas the other site, with fourfold multiplicity, (Mn^{+4}) has almost undistorted coordination. The systematic broadening effect on the magnetic reflections associated with the Mn^{+3} sublattice can be explained by the presence of finely spaced ''magnetic spin-flip'' boundaries, which break the coherence of the Mn^{+3} magnetic sublattice but not that of Mn^{+4}. These structures are likely to coincide with the DC boundaries, which would therefore break the coherence of the orbital ordering but not that of the charge ordering. This constitutes indirect evidence that the charge ordering modulation has the same very long coherence length as that of the Mn^{+4} magnetic sublattice.

[1] G. H. Jonker and J. H. V. Santen, Physica **16**, 337 (1950).

[2] S. Jin, T. H. Tiefel, M. McCormack, and R. A. Fastnacht, Science **264**, 413 (1994).

[3] R. von Helmolt, J. Wecker, B. Holzapfel, L. Schultz, and K. Samwer, Phys. Rev. Lett. **71**, 2331 (1993).

[4] K. Chahara, T. Ohno, M. Kasai, and Y. Kozono, Appl. Phys. Lett. **63**, 1190 (1993).

[5] R. M. Kusters, J. Singleton, D. A. Keen, R. McGreevy, and W. Hayes, Physica B **155**, 362 (1989).

[6] C. Zener, Phys. Rev. **82**, 403 (1951).

[7] P. W. Anderson and H. Hasegawa, Phys. Rev. **100**, 675 (1955).

[8] P.-G. de Gennes, Phys. Rev. **118**, 141 (1960).

[9] P. Schiffer, A. P. Ramirez, W. Bao, and S.-W. Cheong, Phys. Rev. Lett. **75**, 3336 (1995).

[10] E. O. Wollan and W. C. Koehler, Phys. Rev. **100**, 545 (1955).

[11] J. B. Goodenough, Phys. Rev. **100**, 564 (1955).

[12] C. H. Chen and S.-W. Cheong, Phys. Rev. Lett. **76**, 4042 (1996).

[13] P. G. Radaelli, D. E. Cox, M. Marezio, S.-W. Cheong, P. E. Schiffer, and A. P. Ramirez, Phys. Rev. Lett. **75**, 4488 (1995).

[14] The scans of the (202-040) reflections shown in Fig. 4 of Ref. 13 were obtained at this wavelength, not at 0.7015 Å as implied in the text. The PSD data shown in the inset were obtained at 0.7015 Å.

[15] R. B. von Dreele, J. D. Jorgensen, and C. J. Windsor, J. Appl. Cryst. **15**, 581 (1982).

[16] M. A. Gilleo, Acta Crystallogr. **10**, 161 (1957).

[17] This coupling is likely to be provided by the orientation of the two octahedral tilt axes of the $Pnma$ structure with respect to the atomic displacements giving rise to the transverse modulation (see below). With $q=[1/2-\varepsilon,0,0]$, the displacements of the $Mn^{+4}O_6$ octahedra are along the c axis, i.e., perpendicular to both tilt axes.

[18] Z. Jirák, S. Krupička, Z. Šimša, M. Dlouhá, and S. Vratislav [J. Magn. Magn. Mater. **53**, 153 (1985)] proposed essentially the same model for orbital ordering, but their space-group symmetry (*Pbmm*) is not compatible with the tilt pattern of the MnO_6 octahedra.

[19] W. Opechowski and R. Guccione, in *Magnetism*, edited by G. T. Rado and H. Suhl (Academic, New York, 1963), Vol. II A, p. 105.

[20] This calculated value of the coherence length is also consistent with the broadening of the superlattice peaks at 18 K in the x-ray synchrotron data at $\lambda=1.1418$ Å (e.g., 0.2° for the 121 peak).

[21] W. L. McMillan, Phys. Rev. B **14**, 1496 (1976).

[22] A. Le Bail, H. Duroy, and J. L. Fourquet, Mater. Res. Bull. **23**, 447 (1988).